Biophysical Chemistry 138 (2008) 55–62

Contents lists available at ScienceDirect

Biophysical Chemistry

journal homepage: http://www.elsevier.com/locate/biophyschem

Fluorescence studies on the photophysical properties and encapsulation behavior of acetaminophen in different environments

N.S. Moyon, T.S. Singh, Sivaprasad Mitra *

Department of Chemistry, North-Eastern Hill University, NEHU Permanent Campus, Umshing, Shillong-793 022, India

ARTICLE INFO

Article history:
Received 8 July 2008
Received in revised form 2 September 2008
Accepted 3 September 2008
Available online 12 September 2008

Keywords:
Acetaminophen
Fluorescence
Cyclodextrin
Micelles
Proton dissociation

ABSTRACT

A systematic study on the spectroscopy and photophysical properties of widely used analgesic and antipyretic drug acetaminophen (NAPAP) was presented using steady state and time-resolved fluorescence spectroscopy. The results in homogeneous solvents were compared with those in bio-mimicking environments of cyclodextrin and micellar cavities. Extensive theoretical calculations using time dependent density functional theory (TDDFT) were also done to substantiate the spectral assignment as well as to compare the structure and stability of possible hydrogen bonded conformations of NAPAP in aqueous medium. Facile proton dissociation occurs due to extensive charge redistribution in the excited state. The variation in fluorescence yield and the life time of excited state species in cyclodextrin cavities and micellar medium is due to shift in acid-base dissociation equilibrium in these environments.

1. Introduction

Acetaminophen (*N*-acetyl-*p*-amino phenol, NAPAP, more commonly known as paracetamol, structure shown in Scheme 1) is one of the most popular and widely used drugs for the treatment of pain and fever [1]. It is considered safe for human use at a recommended dose; however, acute overdose can cause fatal liver damage [2]. Unlike many other non-steroidal anti-inflammatory drugs (NSAIDs), NAPAP is almost unanimously considered to have no anti-inflammatory activity and does not produce gastrointestinal damage or untoward cardiorenal effects. Early work [3] had suggested that the fever reducing action of NAPAP was due to activity in the brain while its lack of any clinically useful anti-inflammatory action was consistent with a lack of prostaglandin inhibition peripherally in the body. Now, recent research [4,5] has shown the presence of a new, previously unknown cyclooxygenase enzyme COX-3, found in the brain and spinal cord, which is selectively inhibited by NAPAP, and is distinct from the two already known cyclooxygenase enzymes COX-1 and COX-2. It is now believed that this selective inhibition of the enzyme COX-3 in the brain and spinal cord explains the effectiveness of NAPAP in relieving pain and reducing fever without having unwanted gastrointestinal side effects.

Over 100 years after it was first discovered, the mechanism of action of NAPAP is becoming clear only recently. However, very little is known about the photoactivity of NAPAP like many other NSAIDs, where photosensitivity is a commonly overlooked adverse effect [6]. Recent observations indicate that NAPAP contributes adversely towards repairing of UV-induced DNA damage [7,8]. It is concluded that the inhibition of DNA repair may contribute to the clastogenic effects of NAPAP. Further, it was also shown that glutathione depletion is possible in lung cells incubated with therapeutic concentrations of NAPAP in vitro [9]. As glutathione plays an important role in the antioxidant defense of the skin to UVA irradiation, anything that depletes cellular glutathione levels could have detrimental health effects. On the other hand, taking overdose of some of these analgesic drugs is a known cause of nephritic problems. So, there is a continued interest in detection and estimation of these drugs and their metabolites in clinical laboratories [10]. Several techniques were reported in the literature for determination of paracetamol and related compounds [11]. The methods include mainly indirect spectrophotometric titration [12–14], electrokinetic chromatography [15] and flow injection analysis [16] etc. Although fluorescence is known to be one of the best quantitative techniques for assaying biological samples [17], to the best of our knowledge, there is no report on solution phase fluorescence properties of NAPAP available in the literature. Steady-state absorption and emission spectra as well as nanosecond fluorescence decay properties of powdered NAPAP sample was reported by Moreira et al. [18]. However, in pharmaceutical industries, solubility of drugs are often been considered as a major concern. Nowadays, it is well known that biologically relevant heterogeneous media like cyclodextrins (CDs) and/or surfactants (micelles) can act as potential solubilizing agents for organic compounds by forming host–guest complex [19,20]. In this study, we report our observations on fluorescence properties of NAPAP in different homogeneous solvents as well as binding in cyclodextrin and micellar media by steady state and time-resolved fluorescence spectroscopy.

* Corresponding author. Tel.: +91 364 272 2634; fax: +91 364 255 0486.
E-mail addresses: smitra@nehu.ac.in, sivaprasadm@yahoo.com (S. Mitra).

0301-4622/$ – see front matter © 2008 Elsevier B.V. All rights reserved.
doi:10.1016/j.bpc.2008.09.004

2. Experimental details

Acetaminophen (98%) was received from Alfa Aesar. The sample was further purified by repeated crystallization from 50% aqueous ethanol (v/v). The organic solvents used were of spectroscopic grade (>99.5%) as received from Alfa Aesar and, in some cases, from Aldrich Chemical Company. The analytical grade type-II water, also used as solvent, was obtained from Elix 10 water purification system (Millipore India Pvt. Ltd.). Also, analytically pure NaOH and HCl were used (Sisco Research Laboratories Pvt. Ltd. India) for pH variation experiments. Fluorescence experiments in heterogeneous media were carried out in buffer solution of pH 11.2 prepared by mixing 100 ml of 0.05 M Na_2HPO_4 with 12.6 ml of 0.1 M NaOH [21]. The surfactants sodium dodecyl sulfate (SDS), cetyl trimethyl ammonium bromide (CTAB) as well as α- and β-cyclodextrin (CD) were all obtained from Aldrich Chemical Co. and used as received. All experiments were carried out at room temperature (293 K). The sample concentration (~10 μM) was low enough to avoid any aggregation and kept constant during the variation of surfactant and/or CD concentrations.

Steady-state absorption spectra were recorded on a Perkin-Elmer model Lambda25 absorption spectrophotometer. Fluorescence spectra were taken in a Hitachi model FL4500 spectrofluorimeter and all the spectra were corrected for the instrument response function. Quartz cuvettes of 10 mm optical path length received from Perkin-Elmer, USA (part no. B0831009) and Hellma, Germany (type 111-QS) were used for measuring absorption and fluorescence spectra, respectively. In both fluorescence emission and excitation spectra measurements, 5 nm bandpass was used in the excitation and emission side. Fluorescence quantum yields (ϕ_f) were calculated by comparing the total fluorescence intensity (F) under the whole fluorescence spectral range with that of 4-(dimethylamino)cinnamic acid, (ϕ_f^s=0.002 [22]) using the following equation.

$$\phi_f^i = \phi_f^s \cdot \frac{F^i}{F^s} \cdot \frac{1-10^{-A^s}}{1-10^{-A^i}} \cdot \left(\frac{n^i}{n^s}\right)^2 \quad (1)$$

where, A^i and A^s are the optical density of the sample and standard, respectively, and n^i is the refractive index of solvent at 293 K. The relative experimental error of the measured quantum yield was estimated within ±5%. The pH variation experiments were carried out in a Systronics μ-pH system (type 361, resolution 0.01 pH) at constant temperature (293 K).

Details of time-resolved fluorescence measurement is essentially the same as described elsewhere [23]. Briefly, a CW Nd:Vanadate (Vanguard, Spectra Physics, USA) pumped rhodamine 6G dye laser with doubled tunable output was used for exciting the sample at 309 nm. The fluorescence emission was collected at magic angle (54.7°) in a single photon counting mode with a MCP PMT (R2809, Hamamatsu). The instrument response function (IRF, FWHM–40 ps) was calculated using a dilute scattering solution of a diary creamer and by collecting the emission at the excitation wavelength. The experimentally obtained fluorescence decay traces, $I(t)$, were analyzed by non-linear least-square iterative convolution method based on Lavenberg–Marquardt algorithm [24] and expressed as a sum of exponentials

$$I(t) = \sum_i \alpha_i \exp(-t/\tau_i) \quad (2)$$

where, α_i is the amplitude of the ith component associated with fluorescence lifetime τ_i such that $\sum\alpha_i$=1.

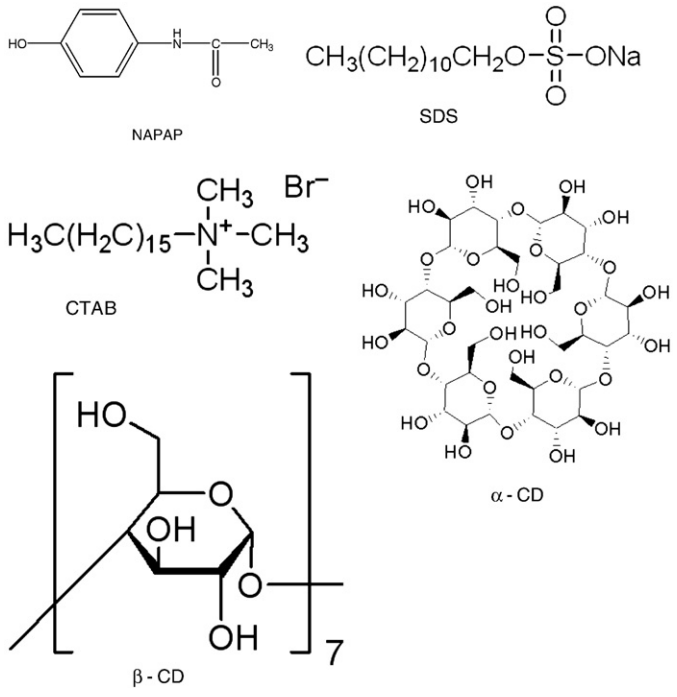

Scheme 1. Structure of acetaminophen (NAPAP) and other complexing agents, viz. sodium dodecyl sulfate (SDS), cetyl trimethyl ammonium bromide (CTAB), α- and β-cyclodextrin (CD) used in this study.

Table 1
Steady-state absorption (λ_{abs}) and fluorescence emission (λ_{fluo}) maxima, Stokes shift ($\Delta\nu_{SS}$) and fluorescence quantum yield (ϕ_f) of NAPAP in different organic solvents

Solvents	λ_{abs}/nm	λ_{fluo}/nm	$\Delta\nu_{SS}$/cm^{-1}	$\phi_f/10^{-3}$
THF	293	324	3265	3.1
ACN	290	322	3427	3.5
DMSO	293	329	3735	2.2
Methanol	290	322	3427	3.7
1-Butanol	290	320	3233	0.7

3. Results and discussion

3.1. Fluorescence properties of acetaminophen in organic solvents: Proton dissociation in excited state

The choice of solvents in which the fluorescence properties of NAPAP can be studied is rather restricted due to the very poor solubility in water. The probe was indeed found to be readily soluble in organic solvents like tetrahydrofuran (THF), acetonitrile (ACN), dimethyl sulfoxide (DMSO) and alcohols. The poor solubility in aqueous medium might be due to the less proton dissociation in NAPAP compared to phenols. Steady-state absorption and fluorescence spectra show a single peak at around 290 nm (with ε~1.13×10^4 M^{-1} cm^{-1} in methanol) and 320 nm respectively with an average Stokes shift of 3400 cm^{-1} (Table 1). None of the absorption and emission spectral peak shows significant shift with solvent polarity, indicating the existence of relatively non-polar neutral (N) structure both in the ground and excited state.

In the presence of the added base, the fluorescence spectra of NAPAP show an additional band in the spectral range of 375–425 nm in different solvents along with the 320 nm peak even on excitation at 290 nm. Fig. 1 shows the representative steady-state spectra in THF. Although the absorption spectrum does not show any appreciable change with added base (data not shown), the excitation spectra corresponding to these emission peaks appear at 330 nm and 290 nm, respectively. Also, excitation at 330 nm shows a single broad emission peak at about 425 nm which resembles very closely to the red emission obtained from 290 nm excitation. Further, addition of more base increases the intensity of 425 nm band with a concomitant decrease in 320 nm fluorescence intensity. All these observations point toward an acid-base equilibrium both in the ground and excited state. The proton dissociated anionic species (A) has the absorption at

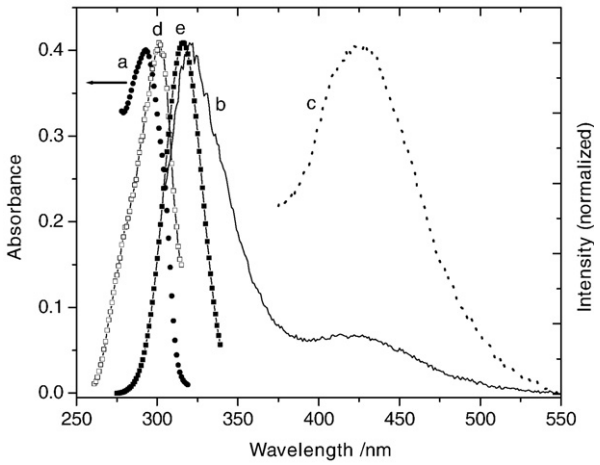

Fig. 1. Steady-state absorption (a) and normalized fluorescence emission (b and c; λ_{exc} = 290 and 320 nm, respectively) spectra of NAPAP (~12 μM) in THF. Normalized fluorescence excitation spectra (d and e; λ_{mon} = 325 and 425 nm, respectively) are also shown.

320 nm and the emission at around 425 nm. These assignments were further confirmed by TDDFT calculations on NAPAP (see below).

3.2. Spectroscopy of acetaminophen in aqueous medium

To understand the binding properties of NAPAP in cyclodextrin and micellar nanocavities, it is imperative to study the fluorescence behavior of the probe in aqueous medium. However, due to poor solubility of NAPAP in water, the aqueous solution could not be prepared directly. First, quantitative amount of methanol stock solution with NAPAP was transferred into 95% (v/v) water. Then the whole mixture was kept on thermostatic water bath for 30 min at 50 °C under constant stirring to evaporate the methanol content. Lastly, the required amount of water was added to make up the final volume.

The photophysical properties of aqueous NAPAP are almost similar to those observed in organic solvents discussed earlier. The acid-base dissociation equilibrium was monitored by observing the change in fluorescence intensity for the neutral (N) and anionic (A) species at 320 and 425 nm, respectively with addition of reagent grade HCl and NaOH in aqueous NAPAP solution. Effectively, this represents a titration curve for the acid functionality of NAPAP shown in Fig. 2. The intersection at pH around 10.2 indicates the proton dissociation constant, pK_a. This data corroborates well with the known pK_a values of NAPAP measured independently [25] as well as with that for substituted *p*-amino phenols, which is of the order of 10.3.

Fluorescence decay behavior of aqueous NAPAP was monitored by picosecond time correlated single photon counting method. Surprisingly, even for a simple molecule like NAPAP, the fluorescence decays monitored at several wavelengths are far from single exponential in nature. Representative fluorescence decay profiles of aqueous NAPAP at pH 11.2 monitored both at 425 and 330 nm are shown in Fig. 3. Visual inspection of the weighted residuals (shown in the upper panel) and reduced chi-square values indicate the necessity three to four exponentials to properly fit the experimentally obtained data points. The individual decay times (τ_i) and its associated amplitudes (α_i) are given in Table 2.

Multiexponential fluorescence decay is quite common for organic heterocycles in solution and it is often difficult to mechanistically assign the various components of the decay. Particularly, for NAPAP in aqueous medium, there are multiple potent hydrogen bonding sites, both in ground and excited state, to give a distribution of different structures with varying fluorescence decay time. Instead of giving too much importance to individual decay components, we define the second order average lifetime (<τ>) of the fluorophore in solution using Eq. (3) to discuss the fluorescence decay behavior.

$$<\tau>=\frac{\sum_i \alpha_i \times \tau_i^2}{\sum_i \alpha_i \times \tau_i} \quad (3)$$

The calculated values are also listed in the last column of Table 2. Radiative and total non-radiative decay parameters were also calculated from Eq. (4) using the quantum yield of fluorescence at 330 and 425 nm.

$$\kappa^r = \phi/<\tau>; \sum \kappa^{nr} = (1-\phi)/<\tau> \quad (4)$$

Based on the steady state and time-resolved fluorescence results discussed above, the kinetic scheme for the excited state proton dissociation of NAPAP can be shown in Scheme 2.

3.3. Hydrogen bonding in aqueous NAPAP: TDDFT calculations

Density functional theory (DFT) have successfully been applied to study the hydrogen bonding in various structures including organic as well as biological model systems [26–29]. Pan et al. used this functional along with 6-31++G(d,p) basis set to verify the extent of specific solvation of formic acid or formate anion model systems with few water molecules [30], whereas, in a recent paper, the effectiveness of DFT calculations to predict the hydrogen bonding strength between different drug molecules and corresponding receptors was investigated [31]. The success of the DFT method in elucidating the complex phenomenon like hydrogen bonding prompts us to use it further in studying the energetic parameters of isolated NAPAP and its complex with water molecules.

In NAPAP molecule, there are several centers (amino nitrogen, phenolic oxygen as well as carbonyl group), which may serve as potent hydrogen bonding sites for the formation of NAPAP-water hydrogen bonded complex. To further elucidate the ground state structure as well as excited state photophysical properties of NAPAP, detail theoretical calculations were performed using time dependent density functional (B3LYP) at TDDFT/6-311G(d,p) level using Gaussian-03 program package [32]. To verify the effect of incorporating the diffuse functions on the basis set, the same calculations were repeated with 6-311++G(d,p) basis set also.

Frequency calculations were done in each point to confirm the stationary state. No substantial differences in the geometrical parameters were found with increased basis set size. Consequently,

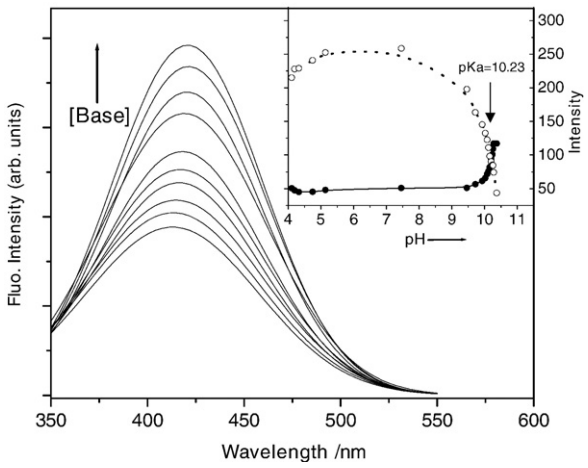

Fig. 2. Increase in proton dissociated anionic emission (A) of aqueous NAPAP with increasing concentration of NaOH (λ_{exc} = 320 nm). Inset shows the variation of emission intensity at 320 nm (open circle) and 425 nm (black circle) with increasing pH of the medium. The intersection indicates the pK_a of the solution.

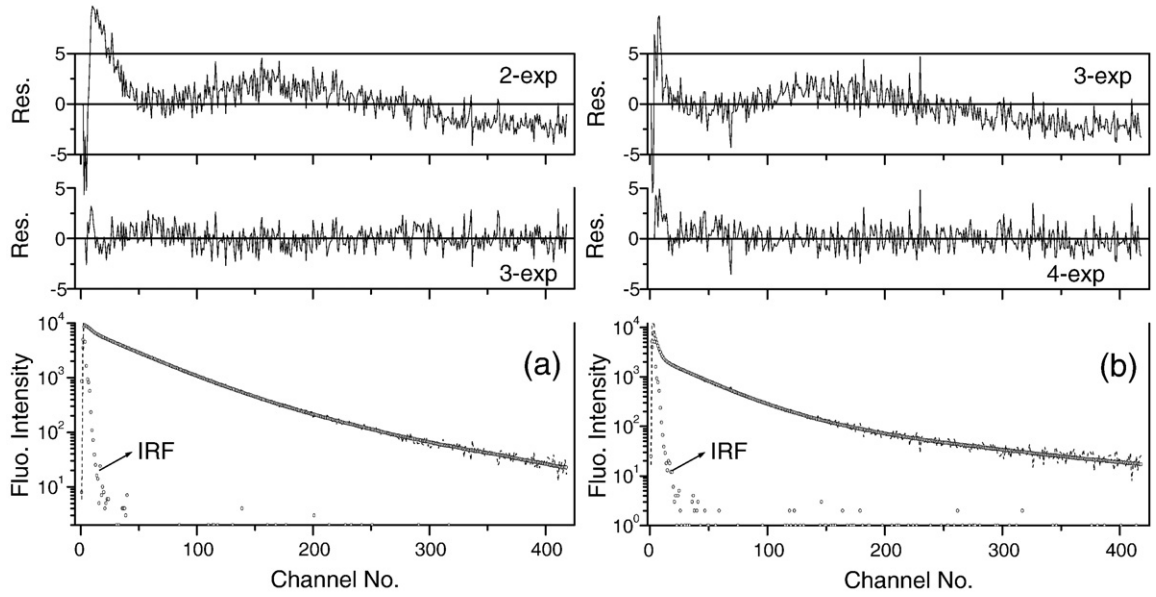

Fig. 3. Typical fluorescence decay curves of aqueous NAPAP monitored at 425 nm (A) and 330 nm (B). Distribution of weighted residuals is shown in the upper panels. The instrument response function (IRF) is shown by dashed line whereas the smooth line indicates the fitting of the experimental data points (time resolution 42.8 ps/channel).

the calculation methodology at (TD)B3LYP/6-311++G(d,p)//6-311G(d,p) was followed throughout this study, i.e. full optimization of different structures were done with 6-311G(d,p) basis set and single point energy calculation with 6-311++G(d,p) basis were used to compare the energetic aspects. Similar methodology was successfully applied recently for characterizing the spectroscopic properties of large organic heterocyclic systems undergoing proton transfer and intramolecular charge transfer on excitation [33,34]. It was also noted that B3LYP method reproduces the experimental results for intramolecularly hydrogen bonded *o*-hydroxy acetophenone derivatives much better than several other hybrid functionals like BHandHLYP, MPWPW91 and MPWB1K etc. [33]. The effect of solvent on the energy parameters was incorporated by self consistent reaction field calculation using polarizable continuum model (SCRF-PCM) developed by Tomasi and coworkers [35].

The fully optimized structure of neutral NAPAP (N), proton dissociated anion (A) and two possible hydrogen bonded (HB) complex of N with water are shown in Scheme 3. All the structural parameters are listed in Table 1S of Supplementary Section. It is to be noted here that primary hydrogen bonded complex with water was considered only on O16 and H14 (see Scheme 3, for numbering) atoms of NAPAP, to give N-HB1 and N-HB2 complexes, respectively. Possibility of HB on N7 site was not considered as the lone pair of electrons is mostly conjugated with the neighboring groups and not available for HB formation. Further, no multiple (simultaneous HB with both H14 and O16 atoms) and/or secondary HB (addition of two more water molecules in one site) formation was considered during the calculation to avoid the time required for these calculation without any significant information relevant to this study.

Table 3 lists the energy parameters, oscillator strength and vertical transition energy for the most intense transition corresponding to N, A, N-HB1 and N-HB2. The formation of the hydrogen bonded complex is thermodynamically favorable; hence it is reasonable to argue that almost all the NAPAP will be in the complexed form. The N-HB2 conformer is more stable by ~6.7 kJ mol^{-1} than N-HB1, so the former can be considered as relatively predominant species in solution. TDDFT calculation predicts all the transitions to be of ππ* type. The lowest energy transition of the deprotonated species (A) is about 3.95 eV (314 nm); whereas, for the nonionic cases, the transition occurs at 4.85 eV (~256 nm). The calculated absorption energy of the anionic form A is in very good agreement with the experimentally obtained value (~320 nm) mentioned before; however, for the neutral species, it does not agree so well. It is to be noted here that while calculating the hydrogen bonded NAPAP–H_2O complex, only a single water molecule was specifically added in different hydrogen bonding sites of NAPAP to give structures N-HB1 and N-HB2. However, it is known that, HB is a long range interaction where a dynamic exchange of various hydrogen bonding partners occurs in several solvation shells around the molecule. So, the discrete hydrogen bonded complex with a single water molecule is an oversimplification of the complex hydrogen bonded network around NAPAP. An ensemble method like molecular dynamics (MD) simulation, in principle, may be applied to determine the complex structure more accurately [36]. However, the results of the present calculation may be sufficient to describe the spectroscopic as well as solubilization behavior of NAPAP in homogeneous and different heterogeneous medium, *at least qualitatively*, as described in the following sections.

Table 2
Fluorescence decay parameters of aqueous NAPAP at pH 11.2

λ_{mon} (nm)	τ_1 (ps)	α_1	τ_2 (ns)	α_2	τ_3 (ns)	α_3	τ_4 (ns)	α_4	$<\tau>$ (ns)
330	70	0.84	1.0	0.08	2.1	0.07	10.4	0.01	3.7
425	<20	0.92	1.58	0.07	3.81	0.01	–	–	1.9[a]

[a] Considering the instrument limited decay of the first component, this time indicates only the upper limit of excited anionic NAPAP species.

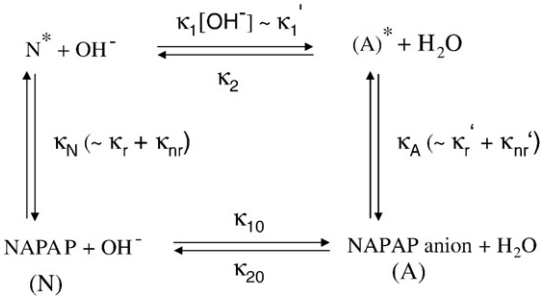

Scheme 2. Proton dissociation and corresponding rate constants of NAPAP in ground and excited states. The neutral and anionic species of NAPAP are represented by N and A, respectively.

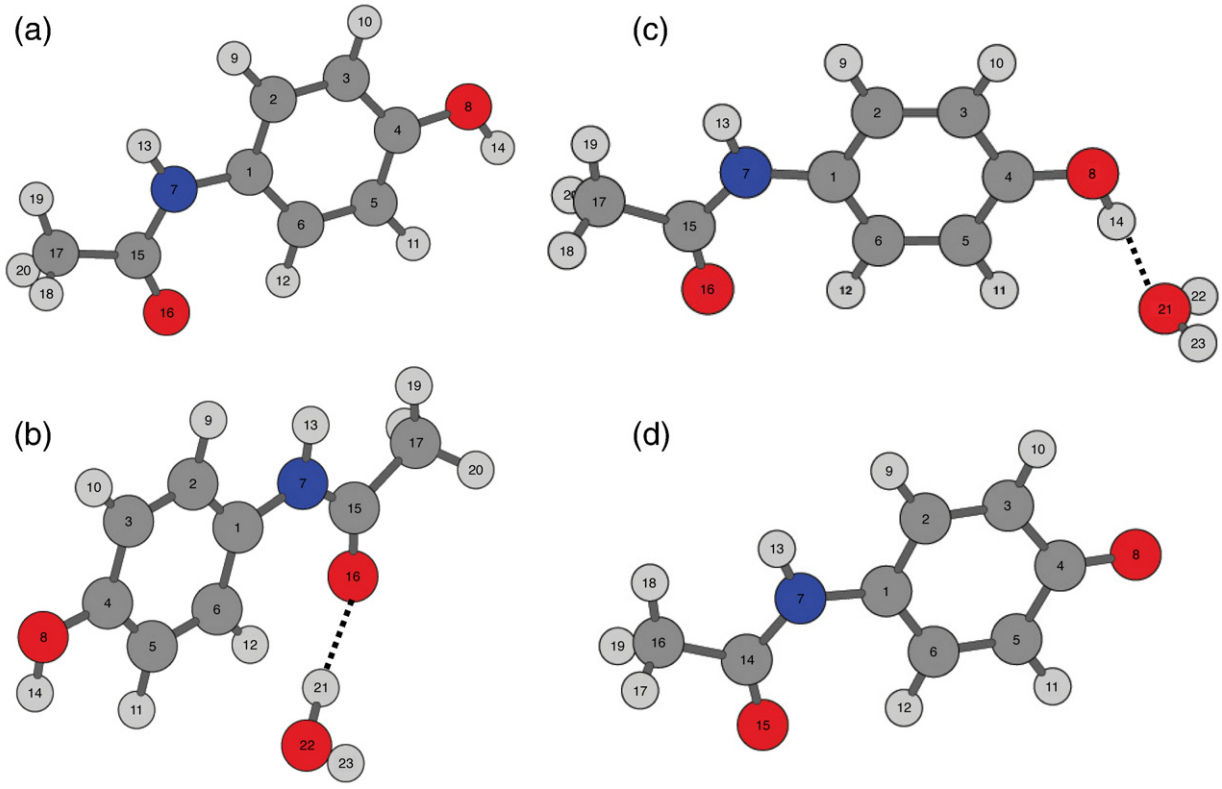

Scheme 3. Fully optimized ground state structures of N(a), N-HB1(b), N-HB2 (c) and A (d) at B3LYP/6-311G(d,p) level of calculation. The atom numbering corresponding to the geometrical parameters given in Table 1S are also shown.

Further, Table 3 indicates that the oscillator strength of A is very small compared with the nonionic species, so it is difficult to identify the anionic species present in solution by absorption spectroscopy, as indeed discussed in the previous section. The calculated dipole moments of both neutral NAPAP as well as the hydrogen bonded complexes are about ~3.5 D, which explains the insensitivity of NAPAP absorption on solvent polarity. A close look into the frontier molecular orbitals (MO), given in Fig. 1S of Supplementary Section, reveals extensive charge redistribution in the excited state. Substantial decrease in electron density over the phenolic group can be regarded as a major reason for facile proton dissociation on excitation.

3.4. Spectroscopy of aqueous acetaminophen in heterogeneous medium

3.4.1. In cyclodextrin

Complexation behavior of aqueous NAPAP was monitored with both α-and β-cyclodextrins (CD) both by steady state and time-resolved fluorescence spectroscopy. It has been observed that absorption intensity increases with increase in the CD concentration without any appreciable change in the spectral peak position. The increase in absorption intensity can be interpreted in terms of greater solubilization of the probe in presence of CDs. However, the fluorescence maxima of both the neutral (N) and anionic (A) species show about 8–10 nm bathochromic shift upon encapsulation inside the CD cavities. Fig. 4 shows the effect of increasing concentration of α-CD on NAPAP fluorescence emission. Similar observations were made with β-CD also.

The stoichiometric ratio and apparent binding constant for NAPAP/CD complex can be determined by analyzing the changes in fluorescence emission with CD concentration. The equilibrium reaction for 1:1 binding between NAPAP and CD can be written as

$$\mathrm{NAPAP} + \mathrm{CD} \overset{K}{\longleftrightarrow} \mathrm{NAPAP{:}CD}. \tag{5}$$

The equilibrium constant for the above process is

$$K = \frac{[\mathrm{NAPAP{:}CD}]_{eq}}{[\mathrm{NAPAP}]_{eq}[\mathrm{CD}]_{eq}}. \tag{6}$$

If the initial concentration of the probe is represented by $[\mathrm{NAPAP}]_0$ and in the condition of $[\mathrm{CD}] \gg [\mathrm{NAPAP}]_0$, Eq. (6) can be reduced to

$$K = \frac{[\mathrm{NAPAP{:}CD}]_{eq}}{\left([\mathrm{NAPAP}]_0 - [NAPAP{:}CD]_{eq}\right)[\mathrm{CD}]}. \tag{7}$$

At any instance, the observed fluorescence intensity (I) is the sum of the fluorescence intensities from the free and bound NAPAP, respectively. Under this condition, one can write

$$I = I_0 \frac{[\mathrm{NAPAP}]_{eq}}{[\mathrm{NAPAP}]_0} + I_\alpha \frac{[\mathrm{NAPAP{:}CD}]_{eq}}{[\mathrm{NAPAP}]_0} \tag{8}$$

Table 3
Calculated ground state energy and singlet excitation parameters for different conformers of NAPAP at TD-B3LYP/6-311G(d,p)//6-311++G(d,p) level

Structure[a]	Transition	Transition energy	Oscillator strength	Type
N (−515.664837)	HOMO→LUMO+1	4.8749 eV (255 nm)	0.52	ππ*
N-HB1 (−592.138349)	HOMO→LUMO	4.8537 eV (256 nm)	0.52	ππ*
N-HB2 (−592.140736)	HOMO→LUMO+1	4.8414 eV (256 nm)	0.53	ππ*
A (−515.180995)	HOMO→LUMO+1	3.9535 eV (314 nm)	0.08	ππ*

Effect of solvent (water) was incorporated using self consistent reaction field (SCRF) in polarized continuum model (PCM) as implemented in Gaussian-03.

[a] Optimized structures are given in Scheme 3; total energies (a.u.) are given in parenthesis.

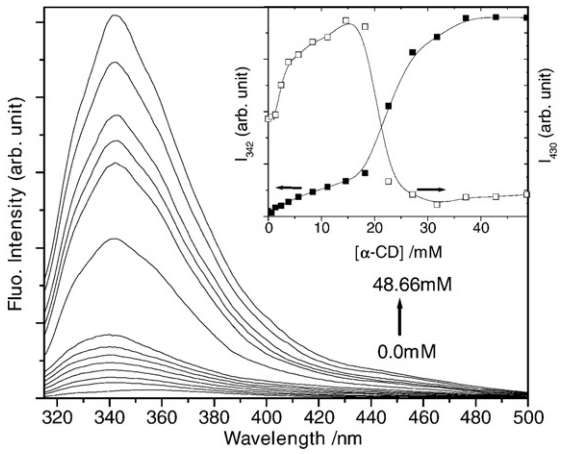

Fig. 4. Change in neutral (N) fluorescence emission (λ_{exc}=290 nm) of aqueous NAPAP with increasing concentration of α-CD. In inset, fluorescence intensity variation at 342 nm (N-emission) and 430 nm (A-emission) are plotted against CD concentration.

where, I_0 and I_α are the fluorescence intensities of the *free* and *fully complexed* NAPAP, respectively. Since, $[NAPAP]=[NAPAP]_{eq}+[NAPAP:CD]_{eq}$, from Eq. (8) we can further write

$$\frac{[NAPAP:CD]_{eq}}{[NAPAP]_0}=\frac{I-I_0}{I_\alpha-I_0}. \tag{9}$$

From Eqs. (6) and (8), the modified form of Benesi–Hilderbrand (BH) relation [37] can be written as

$$\frac{1}{I-I_0}=\frac{1}{I_\alpha-I_0}+\frac{1}{K(I_\alpha-I_0)}\times\frac{1}{[CD]}. \tag{10}$$

Therefore, for 1:1 complex formation, the double reciprocal plot of $1/(I-I_0)$ against $1/[CD]$ should give a straight line; from the slope and intercept of which, the equilibrium constant (K) can be calculated.

In both the cases of α and β-CD, 1:1 complex formation with NAPAP was detected; however, the calculated values for K were very small (ca. 1.6×10^1 M^{-1} and 1.84×10^2 M^{-1} for α- and β-CD, respectively). The small binding constant values indicate inefficient encapsulation of NAPAP in CD cavities. Incorporation of organic probes into the cyclodextrin cavities are mainly controlled by proper fitting of the guest inside host cavity as well as stability of the guest–host complex through hydrophobic interaction [38,39]. DFT calculations, described in the previous section, indicate the presence of N-HB1 as the principle component in aqueous NAPAP. The length of this conformer (9.3 Å) should, *in principle*, fit better in the interior of β-CD cavity (~7.8 Å) compared with that of α-CD (~5.7 Å). In the later case, only a small portion of the molecule can be accommodated into the cavity leaving the rest of the molecule protruding in the bulk. Further, considering the hydrophobic nature of the cyclodextrin cavity, it can be argued that the molecule enters through the *N*-acetyl group towards the cavity to form the host–guest complex.

The variation of normal and anionic NAPAP emission intensity at 342 and 430 nm respectively with increasing concentration of α-CD is shown in the inset of Fig. 4. Interestingly, up to a certain concentration limit of cyclodextrin (~20 mM), both the emission intensities show slight increase. This may be due to greater solubility of the respective species in the cyclodextrin medium. However, beyond that concentration, the intensity of normal emission increases dramatically with a simultaneous decrease in the anionic emission. The sigmoidal shape of the intensity variation curve indicates the establishment of a new acid-base equilibrium in cyclodextrin environment. Compared to the aqueous medium, the proton dissociation is restricted in the relatively hydrophobic cyclodextrin environment. Consequently, the fraction of the anionic species decreases in the solution.

Time-resolved studies on the NAPAP–CD inclusion complexes further supports the observations discussed above. In general, the life time of the excited species increases in CD environment. The decay properties can be explained on the basis of the kinetic scheme (Scheme 2), where, κ_1 and κ_2 are the rate constants for forward and backward proton dissociation process; κ_N and κ_A are the sum of radiative and non-radiative decay rates of the normal (N) and anionic (A) species, respectively. When the rate constants κ_1 and κ_2 are large enough compared with κ_N and κ_A, namely, in the case of fast equilibration between N and A species, the short lifetime component (τ_1 in Table 2) can be approximated as

$$\tau_1\approx\kappa_1+\kappa_2. \tag{11}$$

Because of the overlapping of the N and A emission, it was not possible to determine the κ_1 and κ_2 independently either for free or encapsulated NAPAP, however, increased average lifetime ($\langle\tau\rangle$) of N species in cyclodextrins (Table 4) along with the steady-state fluorescence result discussed above point towards inefficient proton dissociation in cyclodextrin environment. This could be due to the lowering in activation barrier for proton recombination process caused by the destabilization of A in less polar hydrophobic environment in presence of CDs.

3.4.2. In surfactants

Solubilization behavior of aqueous NAPAP was also monitored by steady state and time-resolved fluorescence spectroscopy in anionic (SDS) and cationic (CTAB) surfactants. On addition of surfactants, the absorption spectra do not show significant change; only 3–4 nm red shift is observed along with slight increase in molar extinction coefficient relative to the aqueous medium. However, the fluorescence peak corresponding to the anionic species undergoes a drastic red shift of ~20 nm. This large shift in the fluorescence spectra indicates the passage of the molecules from highly polar aqueous medium to relatively non-polar micellar medium. The passage of molecules towards the micellar cavity can also be demonstrated by the change in NAPAP dissociation equilibrium under micellization. Fig. 5 shows the variation of neutral (N) to anionic (A) fluorescence yield ratio with increase in surfactant concentration. In both the cases an initial sudden reduction in ϕ_N/ϕ_A is observed. The break point appears at approximately 8.1 mM for SDS and 0.5 mM for CTAB which are very close to the CMC of the respective surfactants [40,41]. The sudden reduction in ϕ_N/ϕ_A is explained on the basis of increased solubility of NAPAP on addition of surfactants. Consequently, the content of anion fraction increases in solution and the ratio of ϕ_N/ϕ_A decreases abruptly. However, addition of surfactants beyond CMC results a different pattern for CTAB when compared with SDS; while the ratio of fluorescence yield increases continuously for SDS until it reaches a saturation limit, it decreases in case of CTAB (Fig. 5). This difference can be explained by assuming the location of the probe in micelle–water interface and the electrostatic effect of micellar surface charge on the proton dissociation equilibrium of NAPAP. Since, proton dissociation leads to the formation of NAPAP anion (A), a positive

Table 4
fluorescence quantum yield (ϕ_f), average fluorescence decay time ($\langle\tau\rangle$), radiative (κ^r) and total non-radiative ($\sum\kappa^{nr}$) decay rate constant of neutral and anionic species of NAPAP in different media

	Neutral species (N)				Anionic species (A)			
	ϕ_f (10^{-3})	$\langle\tau\rangle$, ns	κ^r, 10^6 s^{-1}	$\sum\kappa^{nr}$ 10^8 s^{-1}	ϕ_f (10^{-3})	$\langle\tau\rangle$, ns	κ^r, 10^6 s^{-1}	$\sum\kappa^{nr}$ 10^8 s^{-1}
Water	2.1	3.7	0.6	2.7	1.6	1.9	0.8	5.2
α-CD	3.1	4.5	0.7	2.2	4.2	2.5	1.7	4.0
β-CD	3.8	5.9	0.6	1.7	3.7	3.4	1.1	2.9
SDS	7.3	3.5	2.1	2.8	4.5	3.2	1.5	3.1
CTAB	2.9	2.2	1.3	4.5	4.0	3.4	1.2	2.9

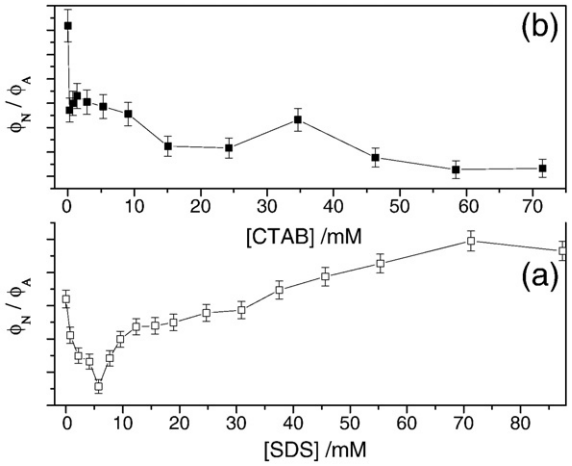

Fig. 5. Variation of ϕ_N/ϕ_A with increasing concentration of SDS (a) and CTAB (b).

micellar surface charge (as in case of CTAB) is expected to favor this process, thereby decreasing the ϕ_N/ϕ_A ratio. Anionic micelle like SDS would behave exactly opposite, as indeed seen in Fig. 5.

Time-resolved fluorescence properties of both N and A forms of NAPAP under fully micellization condition are given in Table 3. In general, it is observed that the fluorescence life time for anionic species increases; however, for the neutral species, although it remains almost same in SDS, there is a substantial decrease in CTAB compared with pure aqueous medium.

4. Conclusions

Photophysical properties of analgesic drug acetaminophen (NAPAP) in homogeneous solution as well as encapsulation behavior in cyclodextrin and micellar environments were reported using steady state and time-resolved fluorescence spectroscopy. The experimental results and extensive theoretical calculation based on time dependent density functional theory (TDDFT) point towards facile proton dissociation and formation of hydrogen bonded complex of NAPAP in aqueous medium. Acid-base dissociation equilibrium is greatly modified in heterogeneous environments. NAPAP forms 1:1 complex both with α- and β-cyclodextrins, whereas, the fluorescence properties indicate the location of the probe in micelle–water interfacial region. Understanding the fluorescence properties in different environments can have direct consequence on biophysical relevance of pharmaceutical and clinical detection of NAPAP in laboratories.

Acknowledgements

This work has been supported by grants received from CSIR (01 (1975)/05/EMR-II) and DST (SR/FTPCS-38/2004), Government of India. The authors thank Professor G. Krishnamoorthy of TIFR, Mumbai and Dr. A. K. Chandra of Dept. of Chemistry, NEHU for allowing us to conduct TCSPC measurements and theoretical calculations in their laboratories, respectively. Support from DST to the Chemistry Department, NEHU through FIST is gratefully acknowledged.

Appendix A. Supplementary data

Supplementary data associated with this article can be found, in the online version, at doi:10.1016/j.bpc.2008.09.004.

References

[1] A. Bertolini, A. Ferrari, A. Ottani, S. Guerzoni, R. Tacchi, S. Leone, Paracetamol: new vistas of an old drug, CNS Drug Review 12 (2006) 250–275.
[2] M. Moore, H. Thor, G. Moore, S. Nelson, P. Moldeus, S. Orrenius, The toxicity of acetaminophen and *N*-acetyl-*p*-benzoquinoneimine in isolated hepatocytes is associated with thiol depletion and increased cytosolic calcium, J. Biol. Chem. 260 (1985) 13035–13040.
[3] R.J. Flower, J.R. Vane, Inhibition of prostaglandin synthetase in brain explains the anti-pyretic activity of paracetamol (4-acetamidophenol), Nature 240 (1972) 410–411.
[4] N.V. Chandrasekharan, H. Dai, K.L.T. Roos, N.K. Evanson, J. Tomsik, T.S. Elton, D.L. Simmons, COX-3, a cyclooxygenase-1 variant inhibited by acetaminophen and other analgesic/antipyretic drugs: cloning, structure, and expression, Proc. Natl. Acad. Sci. USA 99 (2002) 13926–13931.
[5] G.G. Graham, K.F. Scott, Mechanisms of action of paracetamol and related analgesics, Inflammopharmacology 11 (2003) 401–413.
[6] D.E. Moore, Drug-induced cutaneous photosensitivity, Drug Safety 25 (2002) 345–372.
[7] F. Skorpen, B. Alm, C. Skjebred, P.A. Aas, H.E. Krokan, Paracetamol increases sensitivity to ultraviolet (UV) irradiation, delays repair of the UNG-gene and recovery of RNA synthesis in HaCaT cells, Chemico-Biological Interactions 110 (1998) 123–136.
[8] J.K. Hongslo, G. Brunborg, I-L. Steffensen, J.A. Holme, Paracetamol inhibits UV-induced DNA repair in resting human mononuclear blood cells in vitro, Mutagenesis 8 (1993) 423–429.
[9] S. Dimova, P.H.M. Hoet, B. Nemery, Paracetamol (acetaminophen) cytotoxicity in rat type II pneumocytes and alveolar macrophages in vitro, Biochem. Pharmacol. 59 (2000) 1467–1475.
[10] R.M. Welch, A.H. Conney, A simple method for the quantitative determination of *N*-Acetyl-*p*-Aminophenol (APAP) in urine, Clinical Chemistry 11 (1965) 1064–1067.
[11] M.E. Bosch, A.J.R. Sánchez, F.S. Rojas, C.B. Ojeda, Determination of paracetamol: Historical evolution, J. Pharma. Biomed. Anal. 42 (2006) 291–321.
[12] A. Eustaquio, M. Blanco, R.D. Jee, A.C. Moffat, Determination of paracetamol in intact tablets by use of near infrared transmittance spectroscopy, Anal. Chim. Acta 383 (1999) 283–290.
[13] M. de los, A. Oliva, R.A. Olsina, A.N. Masi, Selective spectrofluorimetric method for paracetamol determination through coumarinic compound formation, Talanta 66 (2005) 229–235.
[14] B. Morelli, Spectrophotometric determination of paracetamol in pure form and in tablets, J. Pharma. Biomed. Anal. 7 (1989) 577–584.
[15] T. Németh, P. Jankovics, J. Németh-Palotás, H. Kőszegi-Szalai, Determination of paracetamol and its main impurity 4-aminophenol in analgesic preparations by micellar electrokinetic chromatography, J. Pharma. Biomed. Anal. 47 (2008) 746–749.
[16] J.M. Calatayud, S.S. Vives, An oxidative column for the flow injection analysis — spectrophotometric determination of paracetamol, J. Pharma. Biomed. Anal. 7 (1989) 1165–1172.
[17] J.R. Lackowicz, Principles of Fluorescence Spectroscopy, Springer, Singapore, 2006.
[18] A.B. Moreira, H.P.M. Oliveira, T.D.Z. Atvars, I.L.T. Dias, G.O. Neto, E.A.G. Zagatto, L.T. Kubota, Direct determination of paracetamol in powdered pharmaceutical samples by fluorescence spectroscopy, Anal. Chim. Acta 539 (2005) 257–261.
[19] J. Szejtli, Cyclodextrins in drug formulations, Pharm. Technol. Int. 3 (1991) 15–24.
[20] K. Kano, Y. Ueno, S. Hashimoto, Fluorescence studies on the characterization and solubilizing abilities of sodium dodecyl sulfate, hexadecyltrimethylammonium chloride, and triton X-100 micelles, J. Phys. Chem. 89 (1985) 3161–3166.
[21] R.A. Robinson, R.H. Stokes, Electrolyte Solutions, 2nd ed. rev.Butterworths, London, 1968.
[22] T.S. Singh, S. Mitra, Studies on the binding of 4-(dimethylamino)cinnamic acid with micelles and bovine serum albumin, Photochem. Photobiol. Sci. 7 (2008) 1063–1070.
[23] N. Nag, B.J. Rao, G. Krishnamoorthy, Altered dynamics of DNA bases adjacent to a mismatch: a cue for mismatch recognition by MutS, J. Mol. Biol. 374 (2007) 39–53.
[24] P.R. Bevington, Data reduction and Error Analysis for the Physical Sciences, McGraw-Hill, Inc., New York, 1969.
[25] D.N. Bailey, J.R. Briggs, The binding of acetaminophen, lidocaine, and valproic acid to human milk, Am. J. Clin. Pathol. 121 (2004) 754–757.
[26] J. Mavri, J. Grdadolnik, Proton potential in acetylacetone, J. Phys. Chem. A 105 (2001) 2039–2044.
[27] N. Kobko, L. Paraskevas, E. del Rio, J.J. Dennenberg, Cooperativity in amide hydrogen bonding chains: implication for protein folding models, J. Am. Chem. Soc. 123 (2001) 4348–4349.
[28] L. Bondesson, E. Rudberg, Y. Luo, P. Salek, A linear scaling study of solute–solvent interaction energy of drug molecules in aqua solution, J. Phys. Chem. B 111 (2007) 10320–10328.
[29] L. Benco, D. Tunega, J. Hafner, H. Lischka, Upper limit of O–H···O hydrogen bond. Ab initio study of the kaolinite structure, J. Phys. Chem. B 105 (2001) 10812.
[30] Y. Pan, M.A. McAllister, Characterization of low-barrier hydrogen bonds. 1. Microsolvation effects. An ab initio and DFT investigation, J. Am. Chem. Soc. 119 (1997) 7561–7566.
[31] M.-H. Hao, Theoretical calculation of hydrogen bonding strength for drug molecules, J. Chem. Theory Comput. 2 (2006) 863–872.
[32] M.J. Frisch, et al., Gaussian 03, Revision D.01, Gaussian, Inc., Wallingford CT, 2004.
[33] S. Mitra, T. Sanjoy Singh, A. Mandal, S. Mukherjee, Experimental and computational study on photophysical properties of substituted *o*-hydroxy acetophenone derivatives: Intramolecular proton transfer and solvent effect, Chem. Phys. 342 (2007) 309–317.
[34] T. Sanjay Singh, S. Mitra, A.K. Chandra, N. Tamai, S. Kar, A combined experimental and theoretical study on photoinduced intramolecular charge transfer in *trans*-ethyl *p*-(dimethylamino)cinamate, J. Photochem. Photobiol. A: Chem. 197 (2008) 295–305.

[35] B. Mennucci, J. Tomasi, Continuum solvation models: a new approach to the problem of solute's charge distribution and cavity boundaries, J. Chem. Phys. 106 (1997) 5151–5158.
[36] The authors thank one of the reviewers for bring this point to their notice.
[37] S. Hashimoto, J.K. Thomas, Fluorescence study of pyrene and naphthalene in cyclodextrin–amphiphile complex systems, J. Am. Chem. Soc. 107 (1985) 4655–4662.
[38] W. Saenger, Cyclodextrin inclusion compounds in research and industry, Angew. Chem. Int. Ed. Engl. 19 (1980) 344–362.
[39] K.A. Connors, The stability of cyclodextrin complexes in solution, Chem. Rev. 97 (1997) 1325–1358.
[40] K.J. Mysels, L.H. Princen, Light scattering by some laurylsulfate solutions, J. Phys. Chem. 63 (1959) 1696–1700.
[41] R.S. Sarpal, M. Belletête, G. Durocher, Fluorescence probing and proton-transfer equilibrium reactions in water, SDS, and CTAB using 3,3-dimethyl-2-phenyl-3H-indole, J. Phys. Chem. 97 (1993) 5007–5013.